High photodegradation and antibacterial activity of BN–Ag/TiO 2 composite nanofibers under visible light

M. Nasr, L. Soussan, R. Viter, C. Eid, R. Habchi, Philippe Miele, Mikhael Bechelany

High Photodegradation and Antibacterial Activity of BN-Ag/TiO_2 Composite Nanofibers Under Visible Light

M. Nasr,[a,b] L. Soussan,[a] R. Viter,[c] C. Eid,[b] R. Habchi,[b] P. Miele[a,d] and M. Bechelany†[a]

To develop material with good photocatalytic properties for organic compound degradation and bacterial removal, we produced Ag/TiO_2 and BN-Ag/TiO_2 composite nanofibers that included controlled amounts of boron nitride (BN) nanosheets and silver (Ag). After annealing at 500°C under air, we used scanning electron microscopy, transmission electron microscopy, Brunauer-Emmet-Teller analysis, X-ray diffraction, energy-dispersive X-ray spectroscopy, Raman spectroscopy, UV-visible reflectance spectroscopy and room temperature photoluminescence to investigate the morphological, structural and optical properties of all samples. The photocatalytic tests using methylene blue under visible light, in repeated and long-term applications, showed that the photodegradation activity of BN(5 wt%)-Ag(3 wt%)/TiO_2 composite nanofibers was 17.2 and 2.3 times higher than that of pure TiO_2 and Ag(3 wt%)/TiO_2 nanofibers, respectively. In antibacterial tests using Gram-negative *Escherichia coli*, 3 hours of incubation with BN(5 wt%)-Ag(3 wt%)/TiO_2 composite nanofibers killed all bacteria. These results indicate that the synthesized BN(5 wt%)-Ag(3 wt%)/TiO_2 composite nanofibers can be considered to be multifunctional material for photodegradation and antibacterial applications.

A Introduction

Toxic industrial chemical waste is still not properly treated and may directly pollute drinking water.[1] Therefore, it is urgent to develop effective and economic approaches to remove water contaminants, such as organic pollutants and heavy metal ions.[2] Various methods can be employed to remove biological and chemical pollutants from wastewater, such as photocatalysis, adsorption, filtration and sedimentation.[3, 4] Photocatalysis has gained a great deal of attention as a low cost and environmentally friendly technique because it allows the complete photodegradation of various organic pollutants by using solar energy.[5, 6] Compared with other clean techniques, photocatalysis is a sustainable procedure with strong oxidation ability and lower energy consumption.[7-9] Among the available photocatalysts, titanium dioxide (TiO_2) is one of the most used for environment cleaning purposes due to its chemical stability, low cost, environmental friendliness and strong oxidizing power under ultraviolet light (UV).[10-12] However, the high rate of excited electron-hole recombination of TiO_2 significantly limits the photocatalytic reaction efficiency. In addition, TiO_2 is characterized by a high band gap value (3.2 eV) and consequently can only be excited by UV irradiation, while the solar spectrum mostly consists of visible light (44%) and only a small proportion of UV light (7%). Therefore, TiO_2–based photocatalysis is not efficient when solar light is used as irradiation source.[13] Recently, co-catalysts, such as platinum, silver (Ag), zinc and iron metals or oxides, were loaded on the TiO_2 surface to overcome this problem.[14-17] The metal plays a multi-role in the photocatalytic process by introducing an extrinsic lower band gap, facilitating the separation of electron-hole pairs and hosting catalytically active sites on TiO_2 surface.[1] Among all the noble metals, Ag is promising for extensive applications because of its low cost, easy preparation and antibacterial properties.[18] Many strategies, including chemical reduction, UV irradiation, hydrothermal methods and electrospinning, have been investigated to synthesize different Ag/TiO_2 nanostructures for photocatalytic applications.[14, 19-22] These studies showed that the presence of Ag nanoparticles can largely prevent the recombination of photo-induced electron-hole pairs in TiO_2. Moreover, Ag presence leads to a red shift of TiO_2 absorption edge wavelength, thus enhancing TiO_2 photocatalytic activity under visible light irradiation.

Two-dimensional (2D) boron nitride (BN) nanosheets (white graphene) show structural similarity with graphene and have useful properties, such as high chemical stability and excellent thermal conductivity. BN is an insulator with a wide band gap (up to 5.5 eV, depending on the preparation method). However, recent studies have shown that hexagonal BN (h-BN) have semiconducting and electronic transport properties comparable to those of metals or metal oxides.[23, 24] Moreover, in our previous study we showed in details the impact of BN nanosheets on the photocatalytic activity of TiO_2 nanofibers. We reported that thanks to the electrostatic interaction between BN nanosheets and TiO_2, BN sheets can promote h^+ migration from bulk TiO_2 to its surface and consequently improve TiO_2 photocatalytic activity under UV light due to the efficient charge separation.[25]

Therefore, to develop effective material with photocatalytic properties for both organic compound degradation and bacterial removal, we synthesized Ag/TiO_2 and BN-Ag/TiO_2 composite nanofibers by electrospinning, an easy and cost-effective process for the production of one-dimensional nanostructures from a sol-gel solution with the use of a high electrical field.[26] We prepared exfoliated BN sheets by using an original method based on high-power ultrasonication of BN nanopowder with gelatin.[23] We then analyzed the structural, morphological and optical properties of the prepared samples. Finally, we evaluated their photocatalytic degradation under visible light and antibacterial properties using methylene blue (MB) and *Escherichia coli* cultures, respectively.

B Experimental

1. Materials

Titanium tetraisopropoxide (TTIP) ($Ti[OCH(CH_3)_2]_4$) (97%), polyvinylpyrrolidone (PVP) (Mw = 13,00,000), acetic acid

(98%), absolute ethanol (99%), silver nitrate ($AgNO_3$; 99%), MB, sodium chloride (NaCl, 99%) and gelatin from porcine skin were purchased from Sigma Aldrich. BN nanosheets were obtained from commercial BN (Combat powders, Saint Gobain, 95%, 325 mesh). The *E. coli* (K12 DSM 423) strain was from DSMZ, Germany. Lysogeny broth (LB)-Miller culture medium (ref. n°1214662) was purchased from Fischer Scientific. Ultra-pure water was produced by using the MilliQ system (Millipore). All chemicals were used without any further purification.

2. BN exfoliation

BN nanosheets were obtained by exfoliation of commercial BN powder with gelatin from porcine skin.[23] Briefly, 20g of gelatin was dissolved in 80 ml of hot water (75°C). Then, 1g of BN powder was added to the mixture and the solution was kept in an ultrasonic homogenizer at 50°C overnight. After centrifugation at 6000 rpm for 30 minutes, precipitates (containing exfoliated BN) were dried at 80°C for 48 hours and then calcined in a muffle furnace at 600°C in air for 2 hours to obtain pure exfoliated BN.

3. Preparation of Ag-TiO_2 and BN-Ag/TiO_2 composite nanofibers

Ag/TiO_2 and BN-Ag/TiO_2 composite nanofibers were prepared using the electrospinning technique. The Ag and BN content levels were calculated based on TiO_2 weight percentage (wt. %). The spun solution was prepared in three steps. First, different amounts of $AgNO_3$ (0.5, 1.5 and 3 wt. %) and 2 ml of acetic acid were sonicated for 12h to dissolve $AgNO_3$. Second, TTIP was dissolved in a mixture that contained 5 ml of ethanol and 0.3 g of PVP (precursor solution) and stirred at room temperature for 1h to obtain the viscosity required for electrospinning. Third, dissolved $AgNO_3$ was added to the precursor solution with vigorous magnetic stirring (150 rpm) for 30 min (Ag/TiO_2 solution). A similar Ag/TiO_2 solution but with a fixed Ag content (3 wt. %) was used to prepare BN-Ag/TiO_2 composite nanofibers with specific amounts of exfoliated BN (3 and 5 wt. %). The Ag/TiO_2 or BN-Ag/TiO_2 solution was transferred into a syringe with a stainless steel needle, a diameter of 0.7 mm at a constant flow rate of 1 ml/h. The feeding rate was controlled by the syringe pump. The temperature level inside the electrospinning chamber was 38 ± 5°C. A high voltage power supply was used as source of electric field. Nanofibers were collected on a rotating coil covered with aluminum foil with a rotation speed of 400 rpm. Briefly, the solution was electrospun at a DC voltage of 25 KV and 20 cm working distance (the distance between the needle tip and the collector). As the solution progressed through the system (1 ml/h), it became electrified. The tip of the resulting Taylor cone expelled an electrified jet of fibers, forming a fibrous mesh on the grounded collector.[27] Electrospun Ag/TiO_2 and BN-Ag/TiO_2 composite nanofibers were then calcined in a muffle furnace at 500°C with a heating rate of 5°C/min for 4 hours in air for polymer removal and TiO_2 crystallization. In addition, the annealing process led to the thermal decomposition of $AgNO_3$ to Ag_2O and finally to Ag.[28] Table 1 lists the produced nanofibers tested in this study.

Table 1. TiO_2, Ag/TiO_2 and BN-Ag/TiO_2 samples prepared with different weight amounts of BN nanosheets and $AgNO_3$

Sample name	Sample description	$AgNO_3$ content (%)	BN content (%)
TiO_2	TiO_2	-	-
Ag0.5/TiO_2	Ag(0.5 wt%)/TiO_2	0.5	-
Ag1.5/TiO_2	Ag(1.5 wt%)/TiO_2	1.5	-
Ag3/TiO_2	Ag(3 wt%)/TiO_2	3	-
BN3-Ag3/TiO_2	BN(3 wt%)-Ag(3 wt%)/TiO_2	3	3
BN5-Ag3/TiO_2	BN(5 wt%)-Ag(3 wt%)/TiO_2	3	5

4. Chemical and structural characterizations

X-ray diffraction (XRD) measurements were carried out using a PANAlytical Xpert-PRO diffractometer equipped with an X'celerator detector using Ni-filtered Cu-radiation (λ= 1.54 ˚A). Transmission electron microscopy (TEM) images were taken with a PHILIPS-CM 20. Raman spectra were obtained using a Labram 1B instrument (Jobin-Yvon S.A., Horiba, France). Spectra were taken at room temperature using a 659 nm laser line as the excitation source. All Raman spectra were recorded in the range of 100-1500 cm^{-1}. Scanning electron microscopy (SEM) images were taken with a Hitachi S4800, Japan. The average diameter of 100 randomly chosen nanofibers for each sample was measured from SEM images using the Image J1.29X software. Energy-dispersive X-ray spectroscopy analysis (EDX) and elemental mapping were performed with a Zeiss EVO HD15 microscope coupled to an Oxford X-MaxN EDX detector. Optical properties were analyzed by diffuse reflectance (Shimadzu UV-3600). The UV–visible (UV-VIS) absorbance spectra of MB were recorded with a Jasco V-570 UV–VIS-NIR spectrophotometer. Each sample surface area was determined from nitrogen adsorption-desorption isotherms at liquid nitrogen temperature using the Micromeritics ASAP 2010 system (outgassing conditions: 200°C-12h). Room temperature photoluminescence (PL) was measured in the range of 400-700 nm. After excitement with a nitrogen Nd:YAG laser (266 nm, 10 mW, 1 kHz), PL was recorded with an optical fiber spectrometer (Ocean Optics usb2000).

5. Photocatalytic activity

The photocatalytic activity of Ag/TiO_2 and BN-Ag/TiO_2 composite nanofibers was evaluated by monitoring the degradation of MB (used as a reference organic pollutant) under visible light. To this aim, 0.4 g/L of each photocatalyst was added to an aqueous suspension of 20 mg/L MB. After dispersion of the nanofibers by sonication in the dark for 60 min to reach the adsorption–desorption equilibrium, the solution was irradiated with visible light (obtained from a 150W light source with emission wavelength > 400 nm) for 80 minutes. The number of photons hitting the sample in the reactor is equal to ~ 8.1017 photons/second. The distance between the lamp and the solution (10 cm) was the same for all samples and the temperature was kept constant at 25 ± 0.2 °C by circulating water in the cylindrical tube that surrounded the photo-reactor during the entire experiment. Every 20 minutes, an aliquot of 2 ml was taken from each sample and centrifuged at 6000 rpm for 2 min in the dark to clear the supernatant because filtration resulted in the loss of some catalysts by sorption. The centrifuged solutions were analyzed with a UV/VIS spectrometer. MB absorbance spectra (major absorption band around 664 nm) were recorded to

measure the concentration changes over time. After irradiation, the photocatalytic degradation efficiency was calculated using equation 1:

Degradation efficiency (%) = $(C_0 - C)/C_0 \times 100$ (Equation 1)

where C_0 and C are the MB concentrations before and after photo-irradiation, respectively. This equation gives the percentage of MB degradation by the photocatalyst.
BN5-Ag3/TiO_2 photocatalytic activity repeatability was assessed with the same experimental set-up and after each degradation cycle, the catalyst was separated from the MB solution by centrifugation.

6. Antibacterial activity of TiO_2 nanofibers and BN-Ag/TiO_2 composite nanofibers

6.1. Bacterial strain and culture medium. LB-Miller culture medium was used for both liquid and solid bacterial cultures. The non-pathogenic and Gram-negative *E. coli* (K12 DSM 423) strain was selected as model microorganism to assess the samples' antibacterial properties because it is a common indicator of fecal contamination in water.[29]

6.2. Preparation of the bacterial suspensions used for the antibacterial tests. For each test, a new bacterial suspension was prepared from frozen *E. coli* aliquots stored at - 20°C. Aliquots were first rehydrated in LB-Miller medium on a rotary shaker at 110 rpm at 37°C for 3 hours. Then, they were inoculated in fresh LB-Miller medium (5% v/v) and incubated overnight at 37°C under constant stirring (110 rpm) until bacteria reached the stationary growth phase. Bacteria were centrifuged at 10°C at 3000g for 10 minutes to remove nutrients and avoid bacterial growth during the antibacterial test. Bacterial pellets were then suspended in spring water (Cristaline Sainte Cécile, France: $[Ca^{2+}]$ = 39 mg.L^{-1}, $[Mg^{2+}]$ = 25 mg.L^{-1}, $[Na^+]$ = 19 mg.L^{-1}, $[K^+]$ = 1.5 mg.L^{-1}, $[F^-]$ < 0.3 mg.L^{-1}, $[HCO_3^-]$ = 290 mg.L^{-1}, $[SO_4^{2-}]$ = 5 mg.L^{-1}, $[Cl^-]$ = 4 mg.L^{-1}, $[NO_3^-]$ < 2 mg.L^{-1}) to avoid osmotic shock and the suspension absorbance was measured at 600 nm to determine the bacterial concentration, according to calibration curves obtained previously in the laboratory. Bacteria were then diluted in spring water to obtain a bacterial suspension of about 7.0 x 10^8 CFU.mL^{-1}.

6.3. Assessment of the bactericidal properties of TiO_2 and BN5-Ag3/TiO_2 nanofibers. Bactericidal tests were carried out in batch mode, in glass tubes (20mL) equipped with a breathable cap. TiO_2, BN5-Ag3/TiO_2 and BN5-Ag3/TiO_2 nanofibers were diluted to a concentration of 10 mg.mL^{-1} in sterile ultra-pure water in the dark. One mL of bacterial suspension was mixed with 1 mL of spring water and 1 mL of each nanofiber suspension to obtain an initial bacterial concentration (C_0) of 2.3 ± 0.3 x 10^8 CFU.mL^{-1}. After vortexing, samples were incubated at 20°C with constant stirring (110 rpm) on a rotary shaker for 3 hours under normal light (daylight). Controls (1 mL of bacterial suspension, 1 mL of spring water and 1 mL of ultra-pure water without any material) were added to determine the initial bacterial concentration and to check that the vortex step did not affect cell viability.

6.4. Quantification of the bactericidal activity. After the 3-hour incubation with the different nanofiber samples, bacteria were counted using the conventional plaque assay method.[30] After decanting for 15 minutes to separate bacteria from the nanofiber-containing supernatant, bacteria were immediately ten-fold diluted in saline solution (0.9% NaCl) to neutralize the effect of any Ag that might have been desorbed, and then spread on agar plates. Negative control was a plate without bacteria. After overnight growth at 37°C, bacterial colonies were counted, knowing that each colony stemmed from one bacterium. All experiments were performed twice and the bacterial concentration in the sample was calculated as the average number of colonies divided by the inoculated volume, with the corresponding dilution factor taken into account. The quantification limit was 25 CFU.mL^{-1}. Changes in the bacterial concentrations were correlated with the bactericidal performance of the tested nanofiber sample. The concentration decrease was expressed as log-removal values, as described in the United States Environmental Protection Agency recommendations.[29] The log-removal value was defined as the logarithm (base 10) ratio of the bacterial concentration C (CFU.mL^{-1}) measured at a given time relative to the initial bacterial concentration C_0 (CFU.mL^{-1}). A log-removal value of -log (C_0) was attributed to the specific case of total removal of viable bacteria.[31] For instance, for an initial concentration C_0 fixed at 1.0 x 10^8 CFU/mL, a log-removal value of -8 corresponded to total removal.

C Results and discussion

1. Morphological and structural properties of Ag/TiO_2 and BN-Ag/TiO_2 composite nanofibers

Pure TiO_2 nanofibers and Ag/TiO_2 and BN-Ag/TiO_2 composite nanofibers, with different amounts of $AgNO_3$ and BN nanosheets, were obtained using the simple electrospinning technique (Table 1).

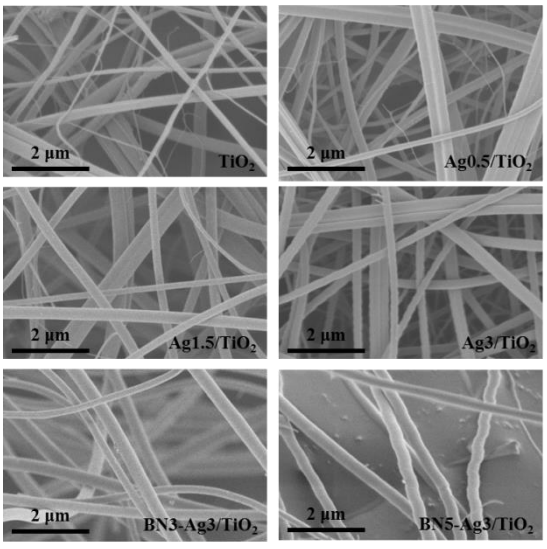

Figure 1. Scanning electron microscope images of pure TiO_2 nanofibers, Ag/TiO_2 and BN-Ag/TiO_2 composite nanofibers after annealing under air at 500°C for 4h.

The Ag content in the TiO_2 nanofibers was adjusted by controlling the amount of $AgNO_3$ in the electrospun solution. After the annealing process at 500°C in air, a very light grayish

tint was observed in samples with increasingly higher Ag content. Conversely, pure TiO_2 nanofibers were white. Analysis of their morphology by SEM (Figure 1) showed the nanofibrous morphology of the obtained Ag/TiO_2 and BN-Ag/TiO_2 composite nanofibers after calcination in air at 500°C for 4 hours. Although the electrospinning parameters were the same for all samples, the average diameter of composite nanofibers calculated from SEM images (Table 2) was significantly higher than that of pure TiO_2 nanofibers. As our previous findings indicate that there is an important relation between the fiber diameter and the dopant content [32], this diameter increase could be attributed to the inclusion of $AgNO_3$ and BN sheets that increase both the total metal content and the viscosity of the electrospinning solution. [33]

EDX was used to study the chemical composition and to confirm the successful production of Ag/TiO_2 and BN-Ag/TiO_2 composite nanofibers. The EDX data (Table 3) revealed the formation of TiO_2 nanofibers with the required atomic ratio of 1:2. For the Ag/TiO_2 composites, the progressive increase of the Ag atom percentage with the $AgNO_3$ content was clearly observed. In BN-Ag/TiO_2 composite nanofibers, the presence of boron progressively increased with the BN nanosheets amount, (taking into account the EDX error 2%). As shown in Table 3, the small amount of carbon residue in the prepared samples arised from the incomplete elimination of PVP during the annealing process at 500°C in air. It is worth to note that due to the overlap between the energy levels of Ti and N (the L energy of Ti and the K energy of N), N could not be detected. Elemental mapping images of a BN3-Ag5/TiO_2 sample (Figure 2) clearly showed that Ti, O, Ag and B elements were well distributed over the entire area of the sample, thus confirming the good dispersion of Ag and BN nanosheets in TiO_2 nanofibers. In conclusion, these data indicate that BN-Ag/TiO_2 composite nanofibers were successfully fabricated using the electrospinning technique.

Table 2. Average diameter of annealed TiO_2, Ag/TiO_2 and BN-Ag/TiO_2 nanofibers

Sample	Average diameter (± 5 nm)
TiO_2	187
$Ag0.5/TiO_2$	192
$Ag1.5/TiO_2$	242
$Ag3/TiO_2$	286
$BN3\text{-}Ag3/TiO_2$	305
$BN5\text{-}Ag3/TiO_2$	319

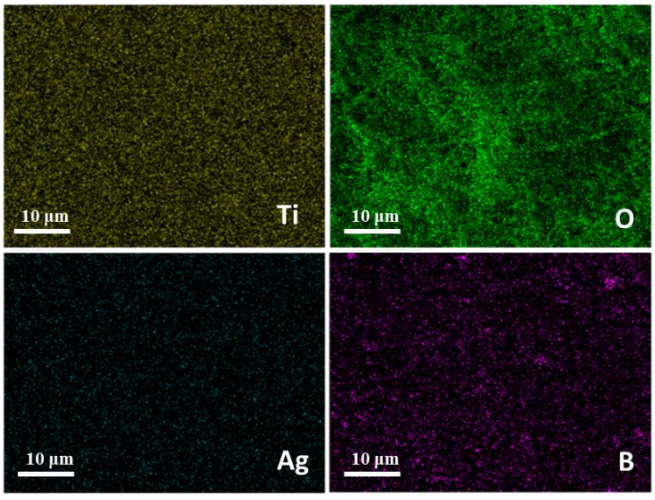

Figure 2. Elemental mapping images of BN5-$Ag3/TiO_2$ composite nanofibers with 5 wt% of BN and 3 wt% of Ag.

Table 3. EDX data showing the composition of annealed TiO_2, Ag/TiO_2 and BN-Ag/TiO_2 nanofibers

	Atomic percentage (± 2 nm)				
	Ti	O	Ag	B	C
TiO_2	32.49	63.76	-	-	3.75
$Ag0.5/TiO_2$	34.46	62.21	0.17	-	3.16
$Ag1.5/TiO_2$	30.47	64.36	0.31	-	4.86
$Ag3/TiO_2$	29.08	64.73	0.70	-	5.49
$BN3\text{-}Ag3/TiO_2$	30.80	60.56	0.72	3.02	4.90
$BN5\text{-}Ag3/TiO_2$	29.15	58.34	0.75	9.16	2.60

Calculation of the surface area of TiO_2, Ag/TiO_2 and BN-Ag/TiO_2 nanocomposites using the Brunauer-Emmet-Teller (BET) method [34] (Table 4) showed that values varied between 19 and 35 m^2g^{-1}. The progressive increase of the surface area with the amount of BN and Ag offers more active adsorption sites and consequently should enhance TiO_2 photocatalytic activity.

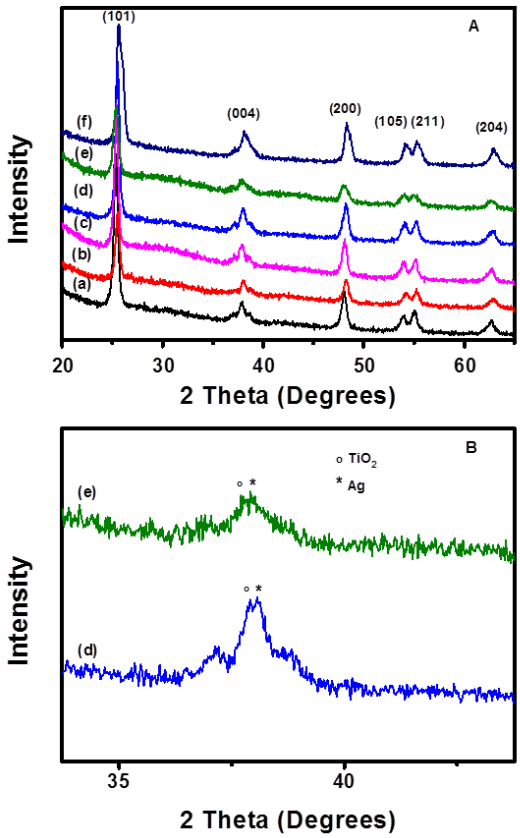

TEM images of pure TiO_2 nanofibers and BN5-$Ag3/TiO_2$ composite nanofibers were used to determine BN and Ag incorporation in TiO_2 nanofibers. Both TiO_2 and BN5-$Ag3/TiO_2$ samples were composed of nanosized grains (Figure S1, supporting information). However, small Ag nanoparticles (black points) were uniformly distributed inside the BN5-$Ag3/TiO_2$ composite nanofibers. We hypothesize that due to the good dispersion of BN in TiO_2 nanofibers, BN sheets could not be detected.

Table 4. Surface area of TiO_2 nanofibers, and Ag/TiO_2 and BN-Ag/TiO_2 composite nanofibers.

Samples	Surface area ($m^2 g^{-1}$)
TiO_2	19.7
$Ag0.5/TiO_2$	19.0
$Ag1.5/TiO_2$	25.5
$Ag3/TiO_2$	31.2
$BN3\text{-}Ag3/TiO_2$	31.8
$BN5\text{-}Ag3/TiO_2$	34.4

Analysis of the XRD spectra of the synthesized TiO_2, Ag/TiO_2 and BN-Ag/TiO_2 nanofibers (Figure 3A) indicated that all spectrum had sharp diffraction peaks located at 2θ = 25.5°, 38.1°, 48.2°, 54.1°, 55.3° and 62.9° relative to the crystal planes of the pure anatase phase of TiO_2 (101), (004), (200), (105), (211) and (204), respectively.[35] The standard peaks of $AgNO_3$ and BN could not be detected by XRD due to their low amount in the samples. However, a small peak of Ag (at 2θ ~ 38°) could be seen in the XRD spectra of $Ag3/TiO_2$ and BN3-$Ag3/TiO_2$ composite nanofibers, indicating Ag presence (Figure 3B).[14, 36] Moreover, the main peak of hexagonal BN (at 2θ ~ 26°) overlapped with the sharp peak of TiO_2 (at 2θ ~ 25.5°). After Ag and BN doping, the diffraction peaks of Ag/TiO_2 and BN-Ag/TiO_2 composite nanofibers were shifted, compared with the peak of pure TiO_2 nanofibers (Figure 3A). We suggest that the slight shifting of the TiO_2 peak is related to peak overlapping between BN and TiO_2. Alternatively, this shift could be due to Ag and BN sheet incorporation that increases the density of surface defects and the lattice strain in the TiO_2 cell, causing vacancy formation as confirmed by PL analysis in our previous study.[25] At the same time, it can shift atoms from the initial position and can reduce the formation of the self-trapped excitons (STE) localized on the TiO_6 octahedral.

According to Bragg's law:[37]

$$n\lambda = 2d \sin\theta \qquad \text{(Equation 2)}$$

the d spacing decreases with the increase of the sinθ value. Therefore, we can say that the d spacing value decreased with the increase of the Ag and BN amounts. This suggests that Ag ions have diffused into the TiO_2 lattice. The average crystal size of TiO_2, Ag/TiO_2 and BN-Ag/TiO_2 samples with different amounts of $AgNO_3$ and BN was estimated using the following Scherrer-Debye equation:[38]

$$D = k\lambda/\beta\cos\theta \qquad \text{(Equation 3)}$$

where D is the average size in nm, k is the shape factor constant (0.9), λ is the X-ray wavelength (0.154 nm), β is the line broadening of the diffraction line measured by the full width at half maximum of the peak intensity (FWHM) and θ is the Bragg angle (in degrees). The results showed that the grain size of the composite nanofibers was higher than that of pure TiO_2 nanofibers (Table 5).

Figure 3. (A-B) XRD spectra of (a) TiO_2, (b) $Ag0.5/TiO_2$, (c) $Ag1.5/TiO_2$, (d) $Ag3/TiO_2$, (e) $BN3\text{-}Ag3/TiO_2$ and (f) $BN5\text{-}Ag3/TiO_2$ nanofibers annealed in air at 500°C for 4h

Table 5. Grain size of annealed TiO_2, Ag/TiO_2 and BN-Ag/TiO_2 nanofibers

	TiO_2	$Ag0.5/TiO_2$	$Ag1.5/TiO_2$	$Ag3/TiO_2$	$BN3\text{-}Ag3/TiO_2$	$BN5\text{-}Ag3/TiO_2$
Grain size (nm)	17.10	18.20	20.40	23.95	22.80	26.15

The formation of BN-Ag/TiO_2 composite nanofibers was further confirmed by Raman spectroscopy. The Raman peaks of all samples at 144 cm^{-1} (E_g), 197 cm^{-1} (E_g), 399 cm^{-1} (B_{1g}), 513 cm^{-1} (A_{1g}), 519 cm^{-1} (B_{1g}) and 639 cm^{-1} (E_g) corresponded to the pure anatase phase of TiO_2 (Figure 4A).[39] The main peak of TiO_2, located at 141 cm^{-1}, was shifted to a larger frequency after Ag and BN doping (Figure S2, supporting information). This frequency shift could be attributed to the pressure effect induced by Ag particles and BN sheets that strongly affects the lattice vibrational characteristics of TiO_2.[40] For BN-Ag/TiO_2 composite nanofibers, a Raman active mode located at ~ 1365 cm^{-1} was identified and was due to hexagonal BN related to the E_{2g} mode (Figure 4B).[41] In addition, an increase in the intensity of the peak corresponding to hexagonal BN with the amount of doping could be clearly observed. No peak related to silver oxide was detected in the Raman and XRD spectra. This confirmed the thermal decomposition of $AgNO_3$ and the formation of Ag nanoparticles.

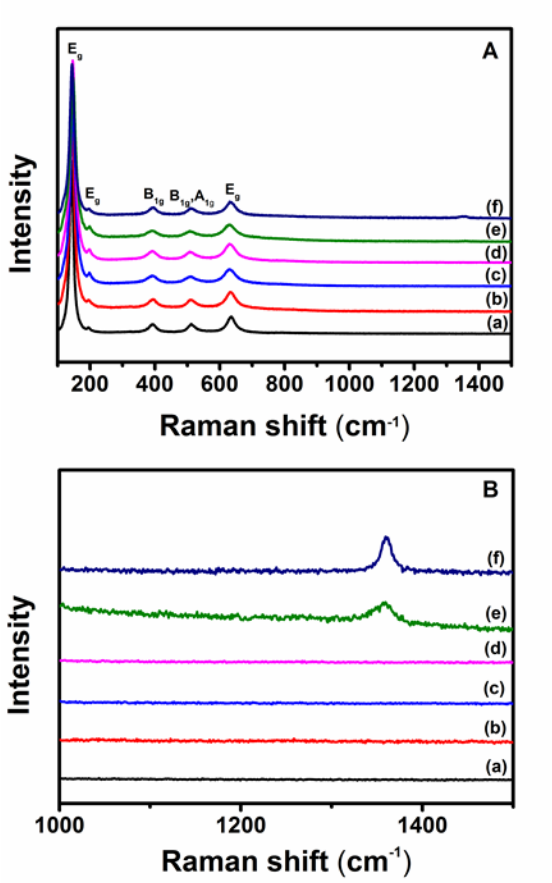

Figure 4. (A-B) Raman shifts of a) TiO_2, (b) $Ag0.5/TiO_2$, (c) $Ag1.5/TiO_2$, (d) $Ag3/TiO_2$, (e) $BN3\text{-}Ag3/TiO_2$ and (f) $BN5\text{-}Ag3/TiO_2$ nanofibers annealed in air at 500°C for 4h

2. Optical properties of TiO_2, Ag/TiO_2 and $BN\text{-}Ag/TiO_2$ composite nanofibers

Incorporation of $AgNO_3$ and BN nanosheets strongly influenced the optical properties of the produced nanofibers. The shift of TiO_2 absorption edges was clearly seen in the reflectance spectra of the different samples (Figure 5). The band gap values of pure TiO_2, Ag/TiO_2 and $BN\text{-}Ag/TiO_2$ composite nanofibers were calculated from the reflectance spectra using the Kubelka–Munk formula:[42]

$$F = \frac{(1-R)^2}{2R} \quad \text{(Equation 4)}$$

$$(Fhv)^{1/2} \sim (hv\text{-}E_g) \quad \text{(Equation 5)}$$

where F, R, hv and E_g represent the Kubelka–Munk function, reflectance, photon energy and band gap, respectively. The E_g values were calculated from the intersection of the linear part of the curve with the hv axis. The fitting was performed automatically using the Origin 9.0 software (Figure 5B). Calculation of the photo-absorption edge wavelengths and band gap values (Figure 5 and Table 6) showed that, compared with pure TiO_2 nanofibers, the absorption edges of Ag/TiO_2 and $BN\text{-}Ag/TiO_2$ composite nanofibers were red-shifted (from 392 to 435 nm) and the band gap values decreased remarkably with the increase of the Ag amount (from 3.16 to 2.85 eV). According to previous studies, this red shift is due to the Ag content because BN has no absorbance edge in the visible range.[43] $Ag3/TiO_2$, BN3- $Ag3/TiO_2$ and BN5-$Ag3/TiO_2$ composite nanofibers had the lowest band gap values. The decrease of TiO_2 band gap value with Ag doping can be explained by the formation of shallow energy states near the conductance band in TiO_2 band gap, as expected when the Ag atoms act like dopants.[44]

Table 6. Photo-absorption edge and band gap values of pure TiO_2 nanofibers, Ag/TiO_2 and $BN\text{-}Ag/TiO_2$ composite nanofibers

Sample	Absorption edge (nm)	Band gap (eV)
TiO_2	392	3.16
$Ag0.5/TiO_2$	413	3.00
$Ag1.5/TiO_2$	417	2.97
$Ag3/TiO_2$	429	2.89
$BN3\text{-}Ag3/TiO_2$	430	2.88
$BN5\text{-}Ag3/TiO_2$	435	2.85

As PL emission results from the recombination of free carriers, PL spectra have been used to investigate the efficiency of charge carrier trapping, migration and transfer in order to understand the fate of electron–hole pairs in semiconductors.[35] In other words, a lower recombination rate or a higher transfer of electrons and holes can result in a lower PL intensity. Many studies have reported PL emissions of pure TiO_2 in photocatalysis research.[45, 46] The PL of BN/TiO_2 nanostructures was investigated for the first time by our group.[25] In this work, we report the PL emission spectra of $BN\text{-}Ag/TiO_2$ nanostructures. As photocatalytic activity improvement is based on the charge separation at the $BN\text{-}Ag/TiO_2$ interface, a lower electron–hole recombination rate in nanocomposites was expected. Consequently, the PL intensity in the $BN\text{-}Ag/TiO_2$ nanostructures should decrease. Analysis of the PL emission spectra of TiO_2, Ag/TiO_2 and $BN\text{-}Ag/TiO_2$ composite nanofibers with different Ag and BN sheets amounts (Figure 6) showed that pure TiO_2 nanofibers had high intensity and broad-band PL signals in the 400–700 nm region, which could be assigned to the radiative recombination of self-trapped excitons (STE).[35] Ag and BN doping significantly reduced the PL intensities of all nanocomposites compared with pure TiO_2 nanofibers. Particularly, the $Ag1.5/TiO_2$, $Ag3/TiO_2$, $BN3\text{-}Ag3/TiO_2$ and $BN5\text{-}Ag3/TiO_2$ samples showed a very weak PL intensity, indicating that they might have the lowest photo-induced electron-hole recombination rate. XRD analysis showed that additional lattice strain appeared in the TiO_2 lattice after BN and Ag doping. This reduces STE formation on the TiO_6 octahedral and therefore, quenches their emission. PL intensity decrease can be mainly explained by the BN and Ag doping effect that leads to the formation of defects on the interface that provide non-radiative recombination and surface charge transfer.[47, 48] The surface charge separation between TiO_2 and BN is expected to improve the photocatalytic activities.[25]

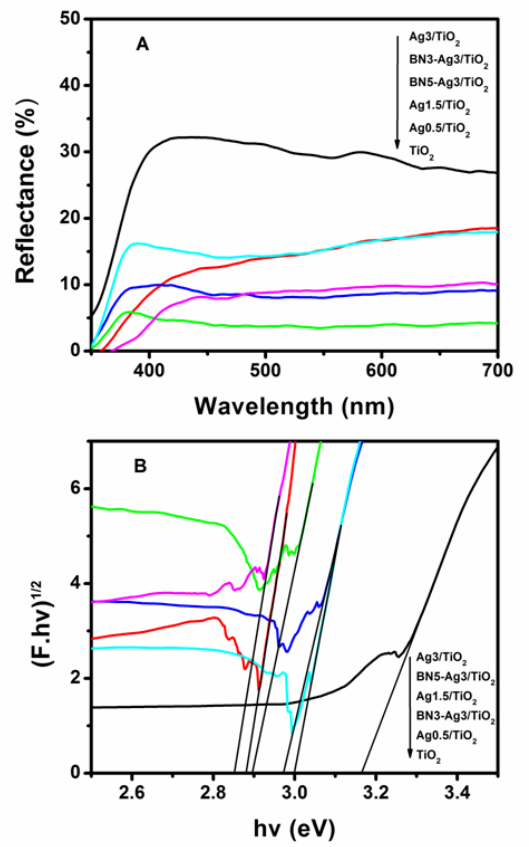

Figure 5. (A) Reflectance spectra and **(B)** Band gap calculation from the reflectance spectra of TiO_2 (black), $Ag0.5/TiO_2$ (cyan), $Ag1.5/TiO_2$ (blue), $Ag3/TiO_2$ (green), $BN3\text{-}Ag3/TiO_2$ (red) and $BN5\text{-}Ag3/TiO_2$ (magenta) composite nanofibers.

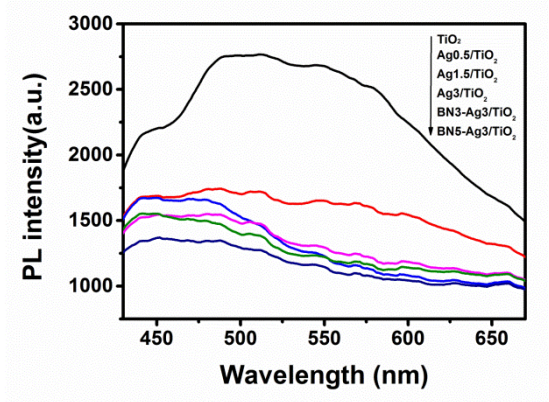

Figure 6. Photoluminescence spectra of pure TiO_2 nanofibers, $Ag0.5/TiO_2$, $Ag1.5/TiO_2$, $Ag3/TiO_2$, $BN3\text{-}Ag3/TiO_2$ and $BN5\text{-}Ag3/TiO_2$ Ag/TiO_2 composite nanofibers.

3. Photocatalytic application

The photocatalytic degradation efficiency of MB by TiO_2, Ag/TiO_2 and $BN\text{-}Ag/TiO_2$ nanofibers with different Ag and BN contents was assessed by calculating the UV–VIS absorbance spectra of the MB solutions (major absorption band around 664 nm) at different time points after exposure to light (0, 20, 40, 60, and 80 min) (Figure 7A for $BN5\text{-}Ag3/TiO_2$). The results obtained with the different nanofibers (Figure 7B) indicated that MB was stable and difficult to be photodegraded under visible light in the absence of photocatalyst. After 80 min of exposure to light, up to 25% of MB was degraded in the presence of pure TiO_2 nanofibers. We previously reported that due to its larger active surface area, the photocatalytic activity of TiO_2 nanofibers is higher than that of commercial TiO_2-P25.[25, 32] The percentage of degraded MB increased gradually with the Ag content: 62% with $Ag0.5/TiO_2$, 73% with $Ag1.5/TiO_2$, and 77% with $Ag3/TiO_2$. It is well accepted that the photocatalytic effect in solid-state catalysis is caused by the electron - hole pairs created from photon adsorption and interaction with molecules close to the catalyst surface.[1] The observed degradation increase could be attributed to the deposition of Ag species onto the surface of TiO_2 nanofibers that can capture the photo-induced electrons and holes. In addition, photo-induced electrons can quickly transfer to the oxygen adsorbed on TiO_2 surface.[18, 47] The improved photocatalytic activity of Ag/TiO_2 composites under visible light compared with pure TiO_2 nanofibers could mainly be ascribed to the lower band gap value, as confirmed by the diffuse reflectance spectra. MB degradation efficiency further increased to 85% with $BN3\text{-}Ag3/TiO_2$ and to 98% with $BN5\text{-}Ag3/TiO_2$ composites. The higher photocatalytic activity of $BN\text{-}Ag/TiO_2$ compared with Ag/TiO_2 composites, with the same amount of Ag, is explained by the efficient electron transfer from photo-excited Ag/TiO_2 to the BN nanosheets of the plasmonic photocatalyst. The efficient charge transfer is related to the pronounced electrostatic interactions. The naturally negatively charged surface of BN sheets could lead to h^+ transfer from the activated Ag/TiO_2 to the BN sheets when they are connected.[49, 50] Therefore, more photo-electrons are available, compared with Ag/TiO_2 samples, to take part in the photodegradation process, in agreement with the photoluminescence analysis.

The kinetic linear curves for all samples are shown in Figure 7C. The photodegradation reactions followed a Langmuir–Hinshelwood first order kinetics model, as described by equation 6:

$$r = dC/dt = kKC/(1+KC) \qquad \text{(Equation 6)}$$

where r is MB degradation rate (mg $(L\ min)^{-1}$), C is the MB solution concentration (mg L^{-1}), t is the irradiation time, k is the reaction rate constant (mg $(L\ min)^{-1}$), and K is MB adsorption coefficient (mg L^{-1}). As the initial concentration (C_0 = 10 mg L^{-1}) of the MB solutions was very low in the present experiments, the relationship between $\ln(C_0/C)$ and the reaction time t showed that MB decomposition with different photocatalysts agreed with a pseudo first-order kinetic:[11]

$$\ln(C_0/C) = kKt = k_a t \qquad \text{(Equation 7)}$$

where ka was the apparent first-order rate constant (min^{-1}) and C the concentration at time t. The obtained k_a values from the linear dependence between $\ln(C_0/C)$ and time are reported in Table 7. The increasing order of the rate constants in the samples was: $BN5\text{-}Ag3/TiO_2$ > $BN3\text{-}Ag3/TiO_2$ > $Ag3/TiO_2$ > $Ag1.5/TiO_2$ > $Ag0.5/TiO_2$ > TiO_2 NFs > MB. The rate constant exhibited a maximum of 0.0465 min^{-1} for $BN5\text{-}Ag3/TiO_2$. This was 17.2 and 2.3 times higher than that of pure TiO_2 nanofibers and $Ag3/TiO_2$ composite nanofibers, respectively. Thus, compared with other samples, $BN5\text{-}Ag3/TiO_2$ nanocomposites showed the highest photocatalytic activity

under visible light, which is represented by their larger k_a value. These results indicate that, compared with TiO_2 and Ag/TiO_2 nanofibers, the coupling effect between BN and Ag/TiO_2 greatly improves the photocatalytic activity under visible light.

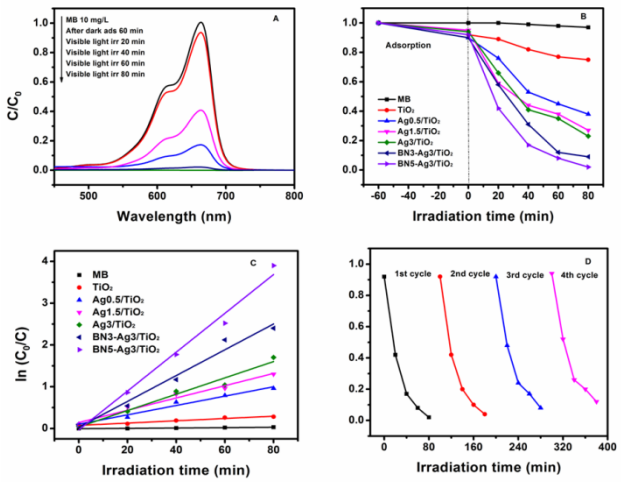

Figure 7. (A) Absorbance spectra of MB degradation in the presence of BN5-Ag3/TiO_2 composite nanofibers. **(B)** MB photodegradation by the TiO_2, Ag/TiO_2 and BN-Ag/TiO_2 photocatalysts under visible light. **(C)** Kinetics of MB degradation**. (D)** Long-term catalytic stability of BN5-Ag3/TiO_2 nanofibers in four repeated cycles of MB degradation under visible light.

Table 7. Kinetic parameters of the photocatalytic activities of pure TiO_2 nanofibers, and Ag/TiO_2 and BN-Ag/TiO_2 composite nanofibers

	k_a (min^{-1})	R^2
MB	0.0004	0.9215
TiO_2	0.0027	0.9544
Ag0.5/TiO_2	0.0112	0.9707
Ag1.5/TiO_2	0.0147	0.9581
Ag3/TiO_2	0.0195	0.9622
BN3-Ag3/TiO_2	0.0309	0.9686
BN5-Ag3/TiO_2	0.0465	0.9819

The catalyst stability has always been the critical issue for long-term repeated use in practical applications.[51] Previous studies reported that TiO_2 nanofibers and Ag/TiO_2 composite nanofibers show high stability in photocatalytic repeatability experiments.[47, 52] Assessment of the photocatalytic activity repeatability in the same conditions showed that MB degradation by BN5-Ag3/TiO_2 composites remained high after four cycles (Figure 7D). This indicates that BN5-Ag3/TiO_2 is stable during the photocatalytic reaction. Also, the used nanofibers had the same light grey color as newly prepared samples. These results confirm that BN5-Ag3/TiO_2 nanofibers have higher photodegradation efficiency compared with pure TiO_2 nanofibers and Ag/TiO_2 composites and long-term stability in photocatalytic activity repeatability tests. As the experimental conditions are different, the photocatalytic activities of BN5-Ag3/TiO_2 composite nanofibers could be only broadly compared with those of previously described Ag/TiO_2 composites (Table S1, supporting information). Nevertheless, BN5-Ag3/TiO_2 composite nanofibers showed the best visible-light photocatalytic activity compared with the other Ag/TiO_2 composites.[14, 18, 47, 53-56]

4. Antibacterial properties

Besides their photocatalytic properties to degrade toxic organic compounds, BN-Ag/TiO_2 nanofibers should also have antibacterial effects. Antibacterial tests were carried out in liquid phase instead of using the disc diffusion method (agar phase) to favor contact [57] between *E. coli* bacteria and TiO_2 nanofibers and BN5-Ag3/TiO_2 composites (under visible light and in the dark). Control reactions without nanofibers showed that bacteria remained viable for 3 hours in the tested conditions (Table 8). Similarly, pure TiO_2 nanofibers had no bactericidal or adsorption effect after 3 hours of contact time under visible light (taking into account the error of 1 Log).[31] On the other hand, total *E. coli* removal (-8 log) was observed with BN5-Ag3/TiO_2 under visible light (day light), while in the dark no antibacterial activity was detected. This indicates that despite the Ag amount (3 wt. %) in the composite, Ag has no bactericidal effect. This can be explained by the fact that Ag is not deposited on the TiO_2 surface, but incorporated in the nanofibers, and thus cannot diffuse to the bacteria. In fact, we suppose that some Ag particles are on the surface of the nanofibers but their amount is not enough to have an antibacterial effect. By comparing the results obtained with BN5-Ag3/TiO_2 under visible light and in the dark (Table 8), it can be concluded that BN sheets have no antibacterial effect in the tested conditions.[58] Therefore, the high antibacterial efficiency of BN5-Ag3/TiO_2 composite nanofibers can be attributed to the stronger photocatalytic activity of TiO_2 under visible light due to Ag and BN doping, in agreement with the photocatalytic results. This study, thus, highlights the strong bactericidal activity of BN5-Ag3/TiO_2 composite nanofibers under visible light. Moreover, the total removal of bacteria (Table 8) and MB (Fig. 7) by BN5-Ag3/TiO_2 under visible light demonstrates the good agreement between antibacterial activity and MB degradation.

Table 8. *E. coli* log-removal values after incubation with pure TiO_2 nanofibers or BN5-Ag3/TiO_2 composite nanofibers at 20°C for 3 hours ($C_0 = 2.3 \pm 0.3 \times 10^8$ CFU.mL^{-1}).

Samples	Removal (Log-values)
Control (3h)	0 ± 1
Pure TiO_2 (Light)	0 ± 1
BN5-Ag3/TiO_2 (Light)	-8 ± 1
BN5-Ag3/TiO_2 (Dark)	0 ± 1

Conclusions

This study shows that Ag/TiO_2 and BN-Ag/TiO_2 composite nanofibers with different amounts of Ag and BN nanosheets can be successfully prepared using the electrospinning

technique. After annealing at 500°C, SEM images show an increase of the average diameter of the composite nanofibers compared with pure TiO_2 nanofibers. TEM images, EDX data and Raman spectra confirm the incorporation of Ag and BN nanosheets in TiO_2 nanofibers. BET measurements and XRD data show the higher specific surface area and grain size of BN-Ag/TiO_2 nanofibers compared with Ag/TiO_2 and TiO_2 nanofibers, respectively. The red shift of the absorbance edge and the decrease of the TiO_2 band gap value from 3.16 to 2.85 eV were confirmed by diffuse reflectance analysis. Ag/TiO_2 and BN-Ag/TiO_2 composites exhibit very weak photoluminescence intensity, and therefore low photo-induced electron-hole recombination compared with pure TiO_2 nanofibers. Moreover, Ag/TiO_2 composite nanofibers have significantly enhanced photocatalytic activity when mixed with BN nanosheets. This higher activity is due to the efficient electron transfer from photo-excited Ag/TiO_2 to BN nanosheets to retard TiO_2 charge recombination. MB degradation efficiency with BN5-Ag3/TiO_2 as catalyst is 17.2 and 2.3 times higher than that of pure TiO_2 nanofibers and Ag3/TiO_2 composites, respectively. Moreover, photocatalytic activity repeatability experiments confirmed the long-term stability of BN5-Ag3/TiO_2 composite nanofibers for MB photodegradation. Antibacterial tests showed that BN5-Ag3/TiO_2 composite nanofibers can kill *E. coli* cultures under visible light, indicating that this effect is related to the enhanced TiO_2 photocatalytic activity upon doping with BN and Ag. In conclusion, the multifunctional BN5-Ag3/TiO_2 composites display photodegradation and antibacterial applications. TiO_2-based photocatalysts doped with Ag and BN nanosheets can be considered as efficient and long-term stable antibacterial materials for biomedical use and water disinfection.

Conflicts of interest

There are no conflicts to declare

Acknowledgements

M. Nasr would like to thank the Lebanese University for PhD funding. This study was partially supported by the ANR project ANR-14-CE07-0011 "BONALD". This research was also supported by the 'Elaboration of metal oxide nanofibers and membranes for photocatalytic applications' project grant attributed to Dr. Cynthia Eid. The authors would like to thank Fabienne WARMONT from Université d'Orléans for TEM images.

Notes and references

1. J. Chen, F. Qiu, W. Xu, S. Cao and H. Zhu, Applied Catalysis A: General, 2015, 495, 131-140.
2. L. Jiang, Y. Huang and T. Liu, Journal of colloid and interface science, 2015, 439, 62-68.
3. M.-V. Sofianou, M. Tassi, V. Psycharis, N. Boukos, S. Thanos, T. Vaimakis, J. Yu and C. Trapalis, Applied Catalysis B: Environmental, 2015, 162, 27-33.
4. C. Chen, W. Ma and J. Zhao, Chemical Society Reviews, 2010, 39, 4206-4219.
5. Z. Wei, Y. Li, S. Luo, C. Liu, D. Meng, M. Ding and G. Zeng, Separation and Purification Technology, 2014, 122, 60-66.
6. L. Zhang, J. Yan, M. Zhou, Y. Yang and Y.-N. Liu, Applied Surface Science, 2013, 268, 237-245.
7. P. Liang, A. Wei, Y. Zhang, J. Wu, X. Zhang and S. Li, Micro & Nano Letters, 2016, 11, 539-544.
8. K. R. Reddy, M. Hassan and V. G. Gomes, Applied Catalysis A: General, 2015, 489, 1-16.
9. T. X. H. Le, M. Bechelany, S. Lacour, N. Oturan, M. A. Oturan and M. Cretin, Carbon, 2015, 94, 1003-1011.
10. S. J. Doh, C. Kim, S. G. Lee, S. J. Lee and H. Kim, Journal of hazardous materials, 2008, 154, 118-127.
11. I. K. Konstantinou and T. A. Albanis, Applied Catalysis B: Environmental, 2004, 49, 1-14.
12. D. H. Kim, H. S. Hong, S. J. Kim, J. S. Song and K. S. Lee, Journal of Alloys and Compounds, 2004, 375, 259-264.
13. L. Cai, Q. Long and C. Yin, Applied Surface Science, 2014, 319, 60-67.
14. M. J. Nalbandian, M. Zhang, J. Sanchez, S. Kim, Y.-H. Choa, D. M. Cwiertny and N. V. Myung, Journal of hazardous materials, 2015, 299, 141-148.
15. C. C. Pei and W. W.-F. Leung, Catalysis Communications, 2013, 37, 100-104.
16. V. Keller, P. Bernhardt and F. Garin, Journal of catalysis, 2003, 215, 129-138.
17. B. Pal, M. Sharon and G. Nogami, Materials Chemistry and Physics, 1999, 59, 254-261.
18. Y.-C. Yao, X.-R. Dai, X.-Y. Hu, S.-Z. Huang and Z. Jin, Applied Surface Science, 2016, 387, 469-476.
19. G. Guo, B. Yu, P. Yu and X. Chen, Talanta, 2009, 79, 570-575.
20. X. He, Y. Cai, H. Zhang and C. Liang, Journal of Materials Chemistry, 2011, 21, 475-480.
21. X. Pan, Y. Zhao, S. Liu, C. L. Korzeniewski, S. Wang and Z. Fan, ACS applied materials & interfaces, 2012, 4, 3944-3950.
22. P. Sangpour, F. Hashemi and A. Z. Moshfegh, The Journal of Physical Chemistry C, 2010, 114, 13955-13961.
23. V. Thangaraj, J. Bussiere, J. M. Janot, M. Bechelany, M. Jaber, S. Subramanian, P. Miele and S. Balme, European Journal of Inorganic Chemistry, 2016.
24. M. Öner, A. Çöl, C. Pochat-Bohatier and M. Bechelany, RSC Advances, 2016, 6, 90973-90981.
25. M. Nasr, R. Viter, C. Eid, R. Habchi, P. Miele and M. Bechelany, New Journal of Chemistry, 2017, 41, 81-89.
26. M. Mansour, M. Bechelany, R. Habchi and C. Eid, Physics Letters A, 2016.
27. C. Eid, E. Assaf, R. Habchi, P. Miele and M. Bechelany, RSC Advances, 2015, 5, 97849-97854.
28. M. K. Seery, R. George, P. Floris and S. C. Pillai, Journal of Photochemistry and Photobiology A: Chemistry, 2007, 189, 258-263.
29. O. Water, EP Agency (ed.), 2012.
30. S. Nagarajan, L. Soussan, M. Bechelany, C. Teyssier, V. Cavaillès, C. Pochat-Bohatier, P. Miele, N. Kalkura, J.-M. Janot and S. Balme, Journal of Materials Chemistry B, 2016, 4, 1134-1141.
31. M.-A. Tartanson, L. Soussan, M. Rivallin, S. Pecastaings, C. V. Chis, D. Penaranda, C. Roques and C. Faur, Applied and environmental microbiology, 2015, 81, 7135-7142.
32. M. Nasr, S. Balme, C. Eid, R. Habchi, P. Miele and M. Bechelany, The Journal of Physical Chemistry C, 2016.
33. N. Sarlak, M. A. F. Nejad, S. Shakhesi and K. Shabani, Chemical engineering journal, 2012, 210, 410-416.
34. K. S. Walton and R. Q. Snurr, Journal of the American Chemical Society, 2007, 129, 8552-8556.
35. M. Nasr, A. A. Chaaya, N. Abboud, M. Bechelany, R. Viter, C. Eid, A. Khoury and P. Miele, Superlattices and Microstructures, 2015, 77, 18-24.
36. O. Akhavan, Journal of colloid and interface science, 2009, 336, 117-124.

37. B. Xin, L. Jing, Z. Ren, B. Wang and H. Fu, The Journal of Physical Chemistry B, 2005, 109, 2805-2809.
38. U. Holzwarth and N. Gibson, Nature Nanotechnology, 2011, 6, 534-534.
39. L. Yang, X. Jiang, W. Ruan, J. Yang, B. Zhao, W. Xu and J. R. Lombardi, The Journal of Physical Chemistry C, 2009, 113, 16226-16231.
40. W. Zhang, Y. He, M. Zhang, Z. Yin and Q. Chen, Journal of Physics D: Applied Physics, 2000, 33, 912.
41. K. Leung, H. Li, Y. Zou, K. Ma, Y. Chong, Q. Ye, W. Zhang, S. Lee and I. Bello, Applied physics letters, 2006, 88, 241922.
42. M. Baitimirova, R. Viter, J. Andzane, A. van der Lee, D. Voiry, I. Iatsunskyi, E. Coy, L. Mikoliunaite, S. Tumenas and K. Załęski, The Journal of Physical Chemistry C, 2016, 120, 23716-23725.
43. Y. Ide, K. Nagao, K. Saito, K. Komaguchi, R. Fuji, A. Kogure, Y. Sugahara, Y. Bando and D. Golberg, Physical Chemistry Chemical Physics, 2015, 18, 79-83.
44. S. Demirci, T. Dikici, M. Yurddaskal, S. Gultekin, M. Toparli and E. Celik, Applied Surface Science, 2016, 390, 591-601.
45. Y. Li, C. Song, Y. Wang, Y. Wei, Y. Wei and Y. Hu, Luminescence, 2007, 22, 540-545.
46. J. Liqiang, Q. Yichun, W. Baiqi, L. Shudan, J. Baojiang, Y. Libin, F. Wei, F. Honggang and S. Jiazhong, Solar Energy Materials and Solar Cells, 2006, 90, 1773-1787.
47. Y. Sui, C. Su, X. Yang, J. Hu and X. Lin, Journal of Molecular Catalysis A: Chemical, 2015, 410, 226-234.
48. N. Jaafar, A. Jalil, S. Triwahyono, J. Efendi, R. Mukti, R. Jusoh, N. Jusoh, A. Karim, N. Salleh and V. Suendo, Applied Surface Science, 2015, 338, 75-84.
49. X. Fu, Y. Hu, Y. Yang, W. Liu and S. Chen, Journal of hazardous materials, 2013, 244, 102-110.
50. C. Tang, J. Li, Y. Bando, C. Zhi and D. Golberg, Chemistry–An Asian Journal, 2010, 5, 1220-1224.
51. M. Nasr, R. Viter, C. Eid, F. Warmont, R. Habchi, P. Miele and M. Bechelany, RSC Advances, 2016, 6, 103692-103699.
52. T. Kawahara, Y. Konishi, H. Tada, N. Tohge, J. Nishii and S. Ito, Angewandte Chemie, 2002, 114, 2935-2937.
53. F. Zhang, Z. Cheng, L. Cui, T. Duan, A. Anan, C. Zhang and L. Kang, RSC Advances, 2016, 6, 1844-1850.
54. D. Yang, Y. Sun, Z. Tong, Y. Tian, Y. Li and Z. Jiang, The Journal of Physical Chemistry C, 2015, 119, 5827-5835.
55. M. L. de Souza and P. Corio, Applied Catalysis B: Environmental, 2013, 136, 325-333.
56. H. Zhang, G. Wang, D. Chen, X. Lv and J. Li, Chemistry of materials, 2008, 20, 6543-6549.
57. R. Goei and T.-T. Lim, Water research, 2014, 59, 207-218.
58. G. Gao, A. Mathkar, E. P. Martins, D. S. Galvão, D. Gao, P. A. da Silva Autreto, C. Sun, L. Cai and P. M. Ajayan, Journal of Materials Chemistry A, 2014, 2, 3148-3154.